Composite Structures 366 (2025) 119208

Contents lists available at ScienceDirect

Composite Structures

journal homepage: www.elsevier.com/locate/compstruct

Exact solutions for the linear hardening elastoplastic model in functionally graded spherical shell

Jun Xie [a], Xiaofan Gou [a,*], Pengpeng Shi [b,c,*]

[a] College of Mechanics and Engineering Science, Hohai University, Nanjing, Jiangsu 211000, China
[b] School of Mathematics and Statistics, Ningxia University, Yinchuan, Ningxia 750021, China
[c] Ningxia Basic Science Research Center of Mathematics, Ningxia Key Laboratory of Interdisciplinary Mechanics and Scientific Computing, Ningxia University, Yinchuan, Ningxia 750021, China

ARTICLE INFO

Keywords:
Linear hardening elastoplastic
Functionally graded materials
Spherical shell
Critical load
Exact solutions

ABSTRACT

As functionally graded materials (FGMs) technology advances, there has been a growing emphasis on the mechanical analysis of FGMs structures. Exceeding the yield strength in FGMs structures often leads to irreversible plastic deformation in localized regions under applied loads. An analysis of the linear hardening elastoplastic model is necessary to assess accurately the load-carrying capacity of these structures. It is assumed that the elastic modulus of FGMs spherical shell varies with the thickness distribution of the structure according to a power function. This paper provides the exact solutions for the linear hardening elastoplastic model in the FGMs spherical shell under mechanical loads, including purely elastic, partially plastic, and fully plastic deformation states. The elastoplastic theory is employed to analyze the linear hardening elastoplastic model, and each deformation state is thoroughly analyzed. A significant contribution of this research is the presentation of comprehensive exact solutions for the linear hardening elastoplastic model in FGMs spherical shell, addressing all deformation regions. The findings demonstrate that the radial variation in material properties significantly influences the elastoplastic model analysis of the FGMs spherical shell. These conclusions are expected to aid in the design of FGMs spherical shells to mitigate yielding under high circumferential stress.

1. Introduction

The progression of composite technology has enabled the development of functionally graded materials (FGMs), a novel class of materials characterized by superior properties and promising applications across various fields. The FGMs provide a continuous transition of properties across spatial coordinates, addressing the issue of property discontinuities found at interfaces in traditional composites [1]. In addition, FGMs offer benefits such as reduced residual stress and enhanced fracture resistance, making them popular in applications like aerospace, civil engineering, biomedical engineering, electronic devices, and pressure vessels [2,3].

In the past thirty years, significant attention has been given to mechanical issues of FGMs annular structures, including annulus, cylindrical, and spherical forms. Thorough stress analysis of FGMs annular structures is essential. Horgan and Chan [4] examined the classic Lamé problem involving a pressurized homogeneous isotropic hollow cylinder or circular disk, specifically focusing on a case where elastic modulus varies solely with the radial coordinate. Researchers [5,6] considered variations in elastic modulus described by power and exponential functions and analyzed the stress distributions in FGMs cylinder and spherical shell. Subsequently, Shi and Xie [7] refined the stress solutions for FGMs structures, addressing and correcting the earlier stress analyses conducted in Ref. [5]. Then, Xie et al. [8] derived displacement and stress solutions for FGMs cylinder and sphere under combined pressure and displacement conditions, validating these with the results of the finite difference method. Comprehensive semi-analytical and numerical analyses have also been conducted for FGMs with varying properties. Shi et al. [9,10], Xie et al. [11] showed that the solution for multi-layered cylinders and spherical shells approaches that of continuously varying FGMs as the number of layers increases. Li et al. [12] used Fredholm integral equations to analyze numerically FGMs spherical shell with arbitrarily varying material parameters. Chen and Lin [13], Wang et al. [14] applied a multi-scale model to arbitrary FGMs hollow cylinders.

In addition, structural safety analysis under complex conditions, including but not limited to thermal loads, which may involve

* Corresponding authors.
E-mail addresses: xfgou@hhu.edu.cn (X. Gou), shipengpeng@xjtu.edu.cn (P. Shi).

https://doi.org/10.1016/j.compstruct.2025.119208
Received 18 January 2025; Received in revised form 9 April 2025; Accepted 14 April 2025
Available online 17 April 2025

temperature variations causing expansion or contraction of materials, and rotational effects, where forces due to spinning or turning can influence the stability and integrity of the structure, has also been thoroughly explored [15–28]. Recently, there has been growing interest in multi-field coupling in functionally graded piezoelectric/piezomagnetic (FGPE/PM) structures. Saadatfar [29] studied the transient response of a hollow cylinder composed of FGPE material under hygrothermal loading. Yaghoobi et al. [30] investigated stress distributions in FGPE cylinders and disks under different loads. Based on differential quadrature and finite difference methods, a multi-field coupling analysis of the FGPE cylinder was presented in Ref. [31]. Shi et al. [32] examined magneto-electro-elastic coupling in FGPE/PM cylinder and sphere structures. Dai and Dai [33] looked into rotating FGPE/PM disks under thermal conditions. Further research has also addressed incompressible soft FGMs hollow cylinders and annular thin disks [34–37]. Not only does the relevant study provide an efficient tool for buckling analysis of FGMs soft structures, but some findings that are unique to the FGMs structures are also highlighted.

The study of the elastoplastic model analysis and load-bearing capacity of various annular structures is essential for assessing structural safety, as it allows researchers to understand how these structures behave under different loading conditions. Initially, significant advancements were made in the elastoplastic behavior of homogeneous materials. Turner [38] applied the Tresca criterion to analyze elastoplastic cylinders using small deformation theory. Grave [39] provided stress solutions for disks by elastoplastic model, whereas Wang et al. [40] investigated critical pressure distributions with full elastic, partial plastic, and complete plastic deformation states. You and Zhang [41] examined elastoplastic responses in rotating solid disks. Rees [42] compared elastoplastic responses in high-speed rotating disks under von Mises and Tresca yield criteria. The elastoplastic deformation model, and linear strain hardening in rotating solid disks under the Tresca criterion and associated flow rules were investigated in Ref. [43]. Bektas [44] derived elastoplastic and residual stress distributions in elastic-perfectly plastic composite disks by the Tsai-Hill yield criterion. A semi-analytical approach for the study of FGMs spherical shell elastoplastic model under thermal and mechanical loads was provided in Ref. [45], where material properties are temperature dependent.

Building on these advancements described above, the elastoplastic analysis of FGMs structures has also progressed. The elastoplastic stresses were derived for the cylinder and rotating FGMs cylinders under internal pressure were derived in Refs. [46,47]. The elastic and plastic deformation states of FGMs pressurized tubes are investigated in the framework of small deformation theory and Tresca's yield criterion in Ref. [48]. Akis and Eraslan [49,50], Eraslan and Akis [51] obtained solutions for rotating FGMs hollow cylinders with constant or power function-varying yield limits. Exact solutions for rotating FGMs thick-walled cylinder [52] and sphere [53], with varying material properties, were derived using both Tresca and von Mises yield criteria. Building on these findings, solutions for FGMs thick cylinders under thermal loading [54] and finite difference numerical solutions [55] were presented. Hassani et al. [56] used Liao's homotropy and finite element method to analyze stress in rotating FGMs disks under thermal loading. Additionally, Atai and Lak [57,58] examined the impact of electric potential on FGMs piezoelectric spheres and cylinders under thermal and pressure loads. Xie et al. [59], Shi and Xie [60] gave the unified displacement and stresses analytical solutions of two different FGMs annular structures in elastoplastic deformation regions under internal pressure in detail.

To the best of our knowledge, the analytical solutions for the linear hardening elastoplastic of the FGMs spherical sphere under internal pressure have not yet been addressed in the current references. The linear hardening elastoplastic model effectively describes the transition process from elastic to plastic deformation while considering the influence of material heterogeneity on mechanical properties. Based on a linear hardening elastoplastic model, this study investigates the unified critical pressures of FGMs spherical structure across various deformation states, including full elasticity, partial elasticity and plasticity, and full plasticity. Importantly, the analysis of FGMs spherical shell in this study begins with an elastic analysis, followed by an elastoplastic analysis. The validity of the analytical solutions is confirmed by comparing them with established results from Refs. [8], [59] and [61]. The paper is organized as follows. The statement and basic equations for the FGMs spherical shell are given in Section 2. Then, analytical solutions of the spherical symmetry elastoplastic model for FGMs spherical sphere are obtained in Section 3. Numerical verifications and discussions are given in Sections 4 and 5, respectively. Some conclusions are obtained finally.

2. Basic equations for FGMs spherical shell

2.1. Statement and basic equations

As shown in Fig. 1, the schematic of the model considered in this paper is given. For the linear hardening elastoplastic model of FGMs structures, elastic modulus is $E_i(r) = E_i(r/b)^{\beta}$ ($i = 0$ and 1) and yield strength is Y_0, where β represents a graded parameter. Fig. 1(b) and 1(c) illustrate the FGMs spherical shell characterized by the radii a and b, respectively. The FGMs structure is under internal pressure p. The analysis is a spherically symmetric problem and the spherical polar coordinate system (r, θ, φ) is used in this paper. Given the symmetry of the problem, the radial displacement $u_r(r)$ is nonzero. It needs to be clarified that when $E_1 = 0$, the model considered in this paper degenerates into an ideal elastoplastic model.

As illustrated in Fig. 2, the deformations of FGMs spherical shell are identified: pure elastic, partial plastic deformations from spherical shell inner/outer surface, and full plastic deformation. These are designated as Cases A, B, C, and D. Therefore, the FGMs spherical shell exhibits both elastic and plastic deformation regions for the middle two Cases. Herein, the coordinates marking the interface between different deformation regions of FGMs spherical shell are represented as ρ_1 and ρ_2, respectively.

For Cases A (elastic deformation) and D (plastic deformation), the boundary conditions are as follows

$$\sigma_r|_{r=a} = -p,\ \sigma_r|_{r=b} = 0 \tag{1}$$

where σ_r denotes radial stress.

For Case B (partial plastic deformation from FGMs spherical shell inner surface), boundary and interface continuity conditions are as follows

$$\begin{aligned} &u_r^e(\rho_1) = u_r^p(\rho_1), \sigma_r^e(\rho_1) = \sigma_r^p(\rho_1), \\ &\sigma_\theta^e(\rho_1) = \sigma_\theta^p(\rho_1), \sigma_r^p(a) = -p, \sigma_r^e(b) = 0 \end{aligned} \tag{2}$$

where the superscripts e and p denote the elastic and plastic deformation regions, σ_θ denotes circumferential stress.

For Case C (partial plastic deformation from FGMs spherical shell outer surface)

$$\begin{aligned} &u_r^e(\rho_2) = u_r^p(\rho_2), \sigma_r^e(\rho_2) = \sigma_r^p(\rho_2), \\ &\sigma_\theta^e(\rho_2) = \sigma_\theta^p(\rho_2), \sigma_r^e(a) = -p, \sigma_r^p(b) = 0 \end{aligned} \tag{3}$$

2.2. Elastic solutions

The constitutive equations for FGMs spherical shell are

$$\sigma_r = \frac{E_0(r)}{(1+\nu)(1-2\nu)}((1-\nu)\varepsilon_r + 2\nu\varepsilon_\theta) = \frac{2G_0(r)}{1-2\nu}((1-\nu)\varepsilon_r + 2\nu\varepsilon_\theta) \tag{4}$$

$$\sigma_\theta = \frac{E_0(r)}{(1+\nu)(1-2\nu)}(\nu\varepsilon_r + \varepsilon_\theta) = \frac{2G_0(r)}{1-2\nu}(\nu\varepsilon_r + \varepsilon_\theta) \tag{5}$$

where ν is Poisson's ratio, ε_r and ε_θ are radial and circumferential strains, and

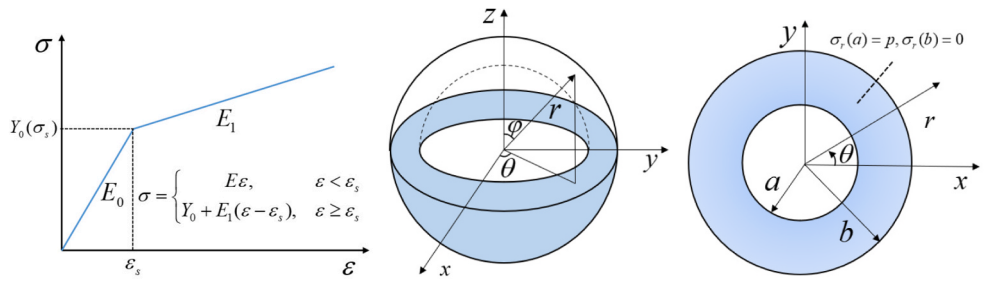

Fig. 1. Schematic of the model considered in this paper, (a) linear hardening elastoplastic model, (b-c) FGMs spherical shell under pressure p.

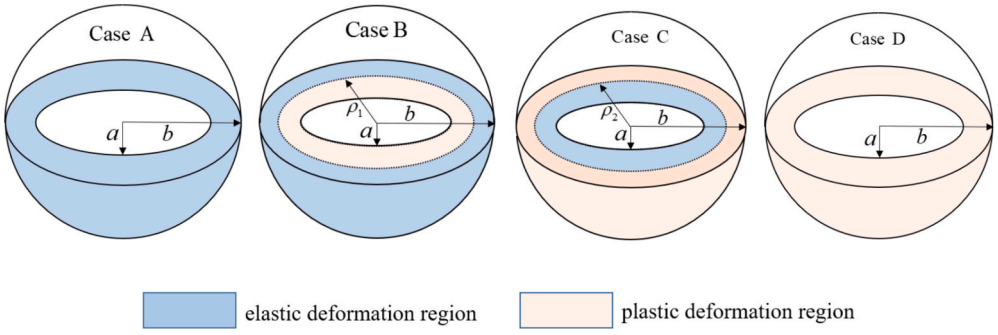

Fig. 2. Elastic and plastic deformation regions for FGMs structures.

$$G_0(r) = \frac{E_0(r)}{2(1+\nu)}$$

The geometric equations are

$$\varepsilon_r = \frac{\mathrm{d}u_r}{\mathrm{d}r}, \varepsilon_\theta = \frac{u_r}{r} \tag{6}$$

The equilibrium equation is

$$\frac{\mathrm{d}\sigma_r}{\mathrm{d}r} + \frac{2(\sigma_r - \sigma_\theta)}{r} = 0 \tag{7}$$

Based on Eqs. (4)-(7), the displacement control equation is obtained as

$$\frac{\mathrm{d}^2 u_r}{\mathrm{d}r^2} + (\beta+2)\frac{\mathrm{d}u_r}{r\mathrm{d}r} + 2(\beta\nu^* - 1)\frac{u_r}{r^2} = 0 \tag{8}$$

where

$$\nu^* = \nu/(1-\nu)$$

The solution of the control equation is

$$u_r = C_1 r^{m_1} + C_2 r^{m_2} \tag{9}$$

where C_1 and C_2 are the undetermined coefficients, and

$$m_{1,2} = \frac{1}{2}\left(-\beta - 1 \pm \sqrt{\beta^2 - 8\beta\nu^* + 2\beta + 9}\right)$$

Substituting Eq. (9) into Eqs. Eq (4)-Eq (6), the stresses solutions for Case A are

$$\sigma_r = g_1 r^{\beta+m_1-1} C_1 + g_2 r^{\beta+m_2-1} C_2 \tag{10}$$

$$\sigma_\theta = g_3 r^{\beta+m_1-1} C_1 + g_4 r^{\beta+m_2-1} C_2 \tag{11}$$

where

$$g_1 = \frac{2G_{00}((m_1-2)\nu - m_1)}{2\nu - 1}, g_2 = \frac{2G_{00}((m_2-2)\nu - m_2)}{2\nu - 1},$$
$$g_3 = -\frac{2G_{00}(\nu m_1 + 1)}{2\nu - 1}, g_4 = -\frac{2G_{00}(\nu m_2 + 1)}{2\nu - 1}, G_{00} = \frac{E_0}{2(1+\nu)}.$$

2.3. Plastic solutions

The stresses and strains satisfy

$$\varepsilon_r^{total} = \frac{\sigma_r(r) - 2\nu\sigma_\theta(r)}{E(r)} + \varepsilon_r^p(r) \tag{12a}$$

$$\varepsilon_\theta^{total} = \varepsilon_\varphi^{total} = \frac{(1-\nu)\sigma_\theta(r) - \nu\sigma_r(r)}{E(r)} + \varepsilon_\theta^p(r) \tag{12b}$$

The incompressible condition is

$$\varepsilon_r^p(r) + \varepsilon_\theta^p(r) + \varepsilon_\varphi^p(r) = 0 \tag{13}$$

then

$$\varepsilon_r^{total}(r) + \varepsilon_\theta^{total}(r) + \varepsilon_\varphi^{total}(r) = \frac{(1-2\nu)(\sigma_r + 2\sigma_\theta)}{E(r)} \tag{14}$$

By combining geometric equations, one can obtain

$$\sigma_r(r) + 2\sigma_\theta(r) = \frac{E(r)}{1-2\nu}\left(\frac{\mathrm{d}u_r(r)}{\mathrm{d}r} + 2\frac{u_r(r)}{r}\right) \tag{15}$$

The yield condition can be written as

$$\sigma_\theta(r) - \sigma_r(r) = 2G_1(r)(\varepsilon_\theta(r) - \varepsilon_r(r)) + Y_0\left(1 - \frac{G_1(r)}{G(r)}\right) \tag{16}$$

where

$$G_1(r) = \frac{E_1(r)}{2(1+\nu)}$$

Combining Eqs. (15) and (16), one can obtain

$$\sigma_r(r) = \frac{(-8\nu+4)G_1(r)+E_0(r)}{3-6\nu}\frac{\mathrm{d}u_r(r)}{\mathrm{d}r} + \frac{2((4\nu-2)G_1(r)+E_0(r))}{3-6\nu}\frac{u_r(r)}{r} - \frac{2Y_0(G_0(r)-G_1(r))}{3G_0(r)} \tag{17}$$

$$\sigma_\theta(r) = \frac{(4\nu-2)G_1(r)+E_0(r)}{3-6\nu}\frac{\mathrm{d}u_r(r)}{\mathrm{d}r} + \frac{2(-2G_1(r)\nu+E_0(r)+G_1(r))}{3-6\nu}\frac{u_r(r)}{r} + \frac{Y_0(G_0(r)-G_1(r))}{3G_0(r)} \tag{18}$$

Substituting Eqs. (17) and (18) into Eq. (7) to obtain the plastic region control equation

$$\frac{\mathrm{d}^2u_r(r)}{\mathrm{d}r^2} + (\beta+2)\frac{\mathrm{d}u_r(r)}{r\mathrm{d}r} - 2\lambda_1\frac{u_r(r)}{r^2} + \lambda_2 r^{-\beta-1} = 0 \tag{19}$$

where

$$\lambda_1 = \frac{((4\nu-2)\beta + 8\nu-4)G_{10}+E_0(\beta-1)}{(8\nu-4)G_{10}-E_0}, \quad \lambda_2 = \frac{6Y_0(2\nu-1)(G_{00}-G_{10})}{G_{00}((-8\nu+4)G_{10}+E_0)}, G_{10} = \frac{E_1}{2(1+\nu)} \tag{20}$$

The displacement in the plastic region is

$$u_r(r) = C_3 r^{m_3} + C_4 r^{m_4} + m_5 r^{-\beta+1} \tag{21}$$

where C_3 and C_4 are the undetermined coefficients, and

$$m_{3,4} = \frac{1}{2}\left(-\beta-1 \pm \sqrt{\beta^2+2\beta+8\lambda_1+1}\right), m_5 = \frac{\lambda_2}{2\beta+2\lambda_1-2} \tag{22}$$

Substituting Eq. (21) into Eqs. (17) and (18) yields the stresses as

$$\sigma_r(r) = C_3k_1r^{\beta+m_3-1} + C_4k_2r^{\beta+m_4-1} + k_3 \tag{23}$$

$$\sigma_\theta(r) = C_3k_4r^{\beta+m_3-1} + C_4k_5r^{\beta+m_4-1} + k_6 \tag{24}$$

where

$$\begin{aligned} k_1 &= \frac{m_3(-8G_{10}\nu+E_0+4G_{10})+8G_{10}\nu+2E_0-4G_{10}}{3-6\nu}, \\ k_2 &= \frac{m_4(-8G_{10}\nu+E_{00}+4G_{10})+8G_{10}\nu+2E_0-4G_{10}}{3-6\nu}, \\ k_3 &= -\frac{2(G_{00}-G_{10})Y_0}{3G_{00}} + \frac{m_5(((-8\nu+4)G_{01}+E_0)\beta-3E_0)}{-3+6\nu}, \\ k_4 &= \frac{m_3(4G_{10}\nu+E_0-2G_{10})-4G_{10}\nu+2E_0+2G_{10}}{3-6\nu}, \\ k_5 &= \frac{m_4(4G_{10}\nu+E_0-2G_{10})-4G_{10}\nu+2E_0+2G_{10}}{3-6\nu}, \\ k_6 &= \frac{(G_{00}-G_{10})Y_0}{3G_{00}} + \frac{m_5(((4\nu-2)G_{10}+E_0)\beta-3E_0)}{-3+6\nu}. \end{aligned} \tag{25}$$

3. Analytical solution

In this subsection, one analytically explores the FGMs spherical shell across various elastoplastic states. This is accomplished by employing fundamental solutions pertinent to both different deformation regions.

3.1. Solutions to Case A

For Case A, based on the following conditions

$$\sigma_r(a) = -p, \sigma_r(b) = 0 \tag{26}$$

The undetermined coefficients C_1 and C_2 are obtained

$$\begin{aligned} C_1 &= -\frac{b^{\beta+m_2-1}p}{g_1(b^{\beta+m_2-1}a^{\beta+m_1-1}-a^{\beta+m_2-1}b^{\beta+m_1-1})}, \\ C_2 &= \frac{b^{\beta+m_1-1}p}{g_2(b^{\beta+m_2-1}a^{\beta+m_1-1}-a^{\beta+m_2-1}b^{\beta+m_1-1})} \end{aligned} \tag{27}$$

Substituting the undetermined coefficients C_1 and C_2 into Eq. (9), the displacement is further obtained as

$$u_r = -\frac{b^{\beta+m_2-1}pr^{m_1}}{g_1(b^{\beta+m_2-1}a^{\beta+m_1-1}-a^{\beta+m_2-1}b^{\beta+m_1-1})} + \frac{b^{\beta+m_1-1}pr^{m_2}}{g_2(b^{\beta+m_2-1}a^{\beta+m_1-1}-a^{\beta+m_2-1}b^{\beta+m_1-1})} \tag{28}$$

Substituting the undetermined coefficients C_1 and C_2 into Eqs. (10) and (11), the stresses are further obtained as

$$\sigma_r = -\frac{b^{\beta+m_2-1}pg_1r^{\beta+m_1-1}}{g_1(b^{\beta+m_2-1}a^{\beta+m_1-1}-a^{\beta+m_2-1}b^{\beta+m_1-1})} + \frac{b^{\beta+m_1-1}pg_2r^{\beta+m_2-1}}{g_2(b^{\beta+m_2-1}a^{\beta+m_1-1}-a^{\beta+m_2-1}b^{\beta+m_1-1})} \tag{29}$$

$$\sigma_\theta = -\frac{b^{\beta+m_2-1}pg_3r^{\beta+m_1-1}}{g_1(b^{\beta+m_2-1}a^{\beta+m_1-1}-a^{\beta+m_2-1}b^{\beta+m_1-1})} + \frac{b^{\beta+m_1-1}pg_4r^{\beta+m_2-1}}{g_2(b^{\beta+m_2-1}a^{\beta+m_1-1}-a^{\beta+m_2-1}b^{\beta+m_1-1})} \tag{30}$$

In Case B, it is observed that the maximum difference between circumferential stress $\sigma_\theta(r)$ and radial stress $\sigma_r(r)$ occurs at the inner surface, where $r = a$. By substituting $r = a$ and defining $\sigma_\theta(a)$-$\sigma_r(a) = Y_0$, the initial critical yield load at which yielding commences on the inner surface of FGMs spherical shell can be determined

$$p_e^B = \frac{Y_0g_1g_2(b^{\beta+m_2-1}a^{\beta+m_1-1}-a^{\beta+m_2-1}b^{\beta+m_1-1})}{g_2(g_1-g_3)b^{\beta+m_2-1}a^{\beta+m_1-1}+g_1(g_4-g_2)b^{\beta+m_1-1}a^{\beta+m_2-1}} \tag{31}$$

In Case C, it is observed that the maximum difference occurs at the outer surface of FGMs spherical shell, where $r = b$. Based on a similar process, the initial critical yield load at which yielding commences on the outer surface is

$$p_e^C = \frac{Y_0g_1g_2(b^{\beta+m_2-1}a^{\beta+m_1-1}-a^{\beta+m_2-1}b^{\beta+m_1-1})}{((g_1-g_3)g_2+(g_4-g_2)g_1)b^{2\beta+m_1+m_2-2}} \tag{32}$$

It is evident that internal pressure p attains the lower of p_e^B and p_e^C mentioned above, the FGMs spherical shell experiences partial plastic deformation. Therefore, the initial yield critical pressure is

$$p_e = \min\{p_e^B, p_e^C\} \tag{33}$$

3.2. Solutions to Case B

For Case B, following boundary conditions in the elastic region are considered

$$\sigma_\theta^e(\rho_1) - \sigma_r^e(\rho_1) = Y_0, \sigma_r^e(b) = 0 \tag{34}$$

The undetermined coefficients C_1 and C_2 are obtained

$$\begin{aligned} C_1 &= \frac{g_2b^{m_2}\rho_1^{1-\beta}Y_0}{-\rho_1^{m_1}g_2(g_1-g_3)b^{m_2}+b^{m_1}\rho_1^{m_2}g_1(g_2-g_4)}, \\ C_2 &= -\frac{g_1b^{m_1}\rho_1^{1-\beta}Y_0}{-\rho_1^{m_1}g_2(g_1-g_3)b^{m_2}+b^{m_1}\rho_1^{m_2}g_1(g_2-g_4)} \end{aligned} \tag{35}$$

Substituting the undetermined coefficients C_1 and C_2 into Eqs. (9)-(11), the solutions in the elastic deformation region of FGMs spherical shell for Case B are further derived as

$$u_r^e(r)=\frac{g_2 b^{m_2}\rho_1^{1-\beta}Y_0 r^{m_1}}{-\rho_1^{m_1}g_2(g_1-g_3)b^{m_2}+b^{m_1}\rho_1^{m_2}g_1(g_2-g_4)}-\frac{g_1 b^{m_1}\rho_1^{1-\beta}Y_0 r^{m_2}}{-\rho_1^{m_1}g_2(g_1-g_3)b^{m_2}+b^{m_1}\rho_1^{m_2}g_1(g_2-g_4)} \tag{36}$$

$$\sigma_r^e(r)=\frac{g_1 r^{\beta+m_1-1}g_2 b^{m_2}\rho_1^{1-\beta}Y_0}{-\rho_1^{m_1}g_2(g_1-g_3)b^{m_2}+b^{m_1}\rho_1^{m_2}g_1(g_2-g_4)}-\frac{g_2 r^{\beta+m_2-1}g_1 b^{m_1}\rho_1^{1-\beta}Y_0}{-\rho_1^{m_1}g_2(g_1-g_3)b^{m_2}+b^{m_1}\rho_1^{m_2}g_1(g_2-g_4)} \tag{37}$$

$$\sigma_\theta^e=\frac{g_3 r^{\beta+m_1-1}g_2 b^{m_2}\rho_1^{1-\beta}Y_0}{-\rho_1^{m_1}g_2(g_1-g_3)b^{m_2}+b^{m_1}\rho_1^{m_2}g_1(g_2-g_4)}-\frac{g_4 r^{\beta+m_2-1}g_1 b^{m_1}\rho_1^{1-\beta}Y_0}{-\rho_1^{m_1}g_2(g_1-g_3)b^{m_2}+b^{m_1}\rho_1^{m_2}g_1(g_2-g_4)} \tag{38}$$

For the plastic region, the following boundary conditions and continuity conditions are considered

$$\sigma_r^p(a)=-p, u_r^e(\rho_1)=u_r^p(\rho_1) \tag{39}$$

The undetermined coefficients C_3 and C_4 are obtained as

$$C_3=\frac{-\rho_1^{m_4}(p+k_3)a^{1-\beta}+k_2 a^{m_4}\left(m_5\rho_1^{1-\beta}-C_1\rho_1^{m_1}-C_2\rho_1^{m_2}\right)}{-\rho_1^{m_3}a^{m_4}k_2+\rho_1^{m_4}a^{m_3}k_1},$$
$$C_4=\frac{\rho_1^{m_3}(p+k_3)a^{1-\beta}-k_1 a^{m_3}\left(m_5\rho_1^{1-\beta}-C_1\rho_1^{m_1}-C_2\rho_1^{m_2}\right)}{-\rho_1^{m_3}a^{m_4}k_2+\rho_1^{m_4}a^{m_3}k_1} \tag{40}$$

The displacement and stresses in the plastic deformation region for Case B are further obtained as

$$u_r^p(r)=\frac{-\rho_1^{m_4}(p+k_3)a^{1-\beta}+k_2 a^{m_4}\left(m_5\rho_1^{1-\beta}-C_1\rho_1^{m_1}-C_2\rho_1^{m_2}\right)}{-\rho_1^{m_3}a^{m_4}k_2+\rho_1^{m_4}a^{m_3}k_1}r^{m_3}+\frac{\rho_1^{m_3}(p+k_3)a^{1-\beta}-k_1 a^{m_3}\left(m_5\rho_1^{1-\beta}-C_1\rho_1^{m_1}-C_2\rho_1^{m_2}\right)}{-\rho_1^{m_3}a^{m_4}k_2+\rho_1^{m_4}a^{m_3}k_1}r^{m_4}+m_5 r^{1-\beta} \tag{41}$$

$$\sigma_r^p(r)=\frac{-\rho_1^{m_4}(p+k_3)a^{1-\beta}+k_2 a^{m_4}\left(m_5\rho_1^{1-\beta}-C_1\rho_1^{m_1}-C_2\rho_1^{m_2}\right)}{-\rho_1^{m_3}a^{m_4}k_2+\rho_1^{m_4}a^{m_3}k_1}k_1 r^{\beta+m_3-1}+\frac{\rho_1^{m_3}(p+k_3)a^{1-\beta}-k_1 a^{m_3}\left(m_5\rho_1^{1-\beta}-C_1\rho_1^{m_1}-C_2\rho_1^{m_2}\right)}{-\rho_1^{m_3}a^{m_4}k_2+\rho_1^{m_4}a^{m_3}k_1}k_2 r^{\beta+m_4-1}+k_3 \tag{42}$$

$$\sigma_\theta^p(r)=\frac{-\rho_1^{m_4}(p+k_3)a^{1-\beta}+k_2 a^{m_4}\left(m_5\rho_1^{1-\beta}-C_1\rho_1^{m_1}-C_2\rho_1^{m_2}\right)}{-\rho_1^{m_3}a^{m_4}k_2+\rho_1^{m_4}a^{m_3}k_1}k_4 r^{\beta+m_3-1}+\frac{\rho_1^{m_3}(p+k_3)a^{1-\beta}-k_1 a^{m_3}\left(m_5\rho_1^{1-\beta}-C_1\rho_1^{m_1}-C_2\rho_1^{m_2}\right)}{-\rho_1^{m_3}a^{m_4}k_2+\rho_1^{m_4}a^{m_3}k_1}k_5 r^{\beta+m_4-1}+k_6 \tag{43}$$

Using the stress continuity condition $\sigma_r^e(\rho_1)=\sigma_r^p(\rho_1)$, one obtains

$$p=\frac{g_1\rho_1^{\beta+m_1-1}C_1+g_2\rho_1^{\beta+m_2-1}C_2-c_3k_1\rho_1^{\beta+m_3-1}-c_4k_2\rho_1^{\beta+m_4-1}-k_3}{\frac{\rho_1^{m_3}a^{1-\beta}k_2\rho_1^{\beta+m_4-1}-\rho_1^{m_4}a^{1-\beta}k_1\rho_1^{\beta+m_3-1}}{-\rho_1^{m_3}a^{m_4}k_2+\rho_1^{m_4}a^{m_3}k_1}} \tag{44}$$

where

$$c_3=\frac{-\rho_1^{m_4}a^{1-\beta}k_3+k_2 a^{m_4}\left(m_5\rho_1^{1-\beta}-C_1\rho_1^{m_1}-C_2\rho_1^{m_2}\right)}{-\rho_1^{m_3}a^{m_4}k_2+\rho_1^{m_4}a^{m_3}k_1}$$
$$c_4=\frac{\rho_1^{m_3}a^{1-\beta}k_3-k_1 a^{m_3}\left(m_5\rho_1^{1-\beta}-C_1\rho_1^{m_1}-C_2\rho_1^{m_2}\right)}{-\rho_1^{m_3}a^{m_4}k_2+\rho_1^{m_4}a^{m_3}k_1} \tag{45}$$

3.3. Solutions to Case C

For Case C, the following boundary conditions in the elastic region are considered

$$\sigma_r^e(a)=-p, \sigma_\theta^e(\rho_2)-\sigma_r^e(\rho_2)=Y_0 \tag{46}$$

The undetermined coefficients C_1 and C_2 are obtained

$$C_1=c_1-pc_{10}, C_2=c_2+pc_{20}, \tag{47a}$$

where

$$c_1=\frac{\rho_2^{1-\beta}a^{m_2}g_2Y_0}{a^{m_1}g_1(g_2-g_4)\rho_2^{m_2}-a^{m_2}\rho_2^{m_1}g_2(g_1-g_3)},$$
$$c_{10}=\frac{\rho_2^{m_2}(g_2-g_4)a^{1-\beta}}{a^{m_1}g_1(g_2-g_4)\rho_2^{m_2}-a^{m_2}\rho_2^{m_1}g_2(g_1-g_3)},$$
$$c_2=\frac{-\rho_2^{1-\beta}a^{m_1}g_1Y_0}{a^{m_1}g_1(g_2-g_4)\rho_2^{m_2}-a^{m_2}\rho_2^{m_1}g_2(g_1-g_3)},$$
$$c_{20}=\frac{\rho_2^{m_1}(g_1-g_3)a^{1-\beta}}{a^{m_1}g_1(g_2-g_4)\rho_2^{m_2}-a^{m_2}\rho_2^{m_1}g_2(g_1-g_3)} \tag{47b}$$

Substituting the undetermined coefficients C_1 and C_2 into Eqs. (9)-(11), the solutions in the elastic deformation region for Case C are further derived as follows

$$u_r^e(r)=(c_1-pc_{10})r^{m_1}+(c_2-pc_{20})r^{m_2} \tag{48}$$

$$\sigma_r^e(r)=g_1 r^{\beta+m_1-1}(c_1-pc_{10})+g_2 r^{\beta+m_2-1}(c_2-pc_{20}) \tag{49}$$

$$\sigma_\theta^e(r)=g_3 r^{\beta+m_1-1}(c_1-pc_{10})+g_4 r^{\beta+m_2-1}(c_2-pc_{20}) \tag{50}$$

For the plastic region, the following boundary conditions and continuity conditions are considered

$$\sigma_r^p(b)=0, u_r^e(\rho_2)=u_r^p(\rho_2) \tag{51}$$

The undetermined coefficients C_3 and C_4 are obtained as

$$C_3=\frac{-b^{1-\beta}\rho_2^{m_4}k_3+b^{m_4}(m_5\rho_2^{1-\beta}-C_1\rho_2^{m_1}-C_2\rho_2^{m_2})k_2}{-\rho_2^{m_3}b^{m_4}k_2+\rho_2^{m_4}b^{m_3}k_1}$$
$$C_4=\frac{b^{1-\beta}\rho_2^{m_3}k_3-b^{m_3}(m_5\rho_2^{1-\beta}-C_1\rho_2^{m_1}-C_2\rho_2^{m_2})k_1}{-\rho_2^{m_3}b^{m_4}k_2+\rho_2^{m_4}b^{m_3}k_1} \tag{52}$$

The displacement and stress in the plastic deformation region for Case C are further obtained as

$$u_r^p(r)=\left(\frac{-b^{1-\beta}\rho_2^{m_4}k_3+b^{m_4}(m_5\rho_2^{1-\beta}-C_1\rho_2^{m_1}-C_2\rho_2^{m_2})k_2}{-\rho_2^{m_3}b^{m_4}k_2+\rho_2^{m_4}b^{m_3}k_1}\right)r^{m_3}+\left(\frac{b^{1-\beta}\rho_2^{m_3}k_3-b^{m_3}(m_5\rho_2^{1-\beta}-C_1\rho_2^{m_1}-C_2\rho_2^{m_2})k_1}{-\rho_2^{m_3}b^{m_4}k_2+\rho_2^{m_4}b^{m_3}k_1}\right)r^{m_4}+m_5 r^{1-\beta} \tag{53}$$

$$\sigma_r^p(r)=\left(\frac{-b^{1-\beta}\rho_2^{m_4}k_3+b^{m_4}(m_5\rho_2^{1-\beta}-C_1\rho_2^{m_1}-C_2\rho_2^{m_2})k_2}{-\rho_2^{m_3}b^{m_4}k_2+\rho_2^{m_4}b^{m_3}k_1}\right)k_1 r^{\beta+m_3-1}+\left(\frac{b^{1-\beta}\rho_2^{m_3}k_3-b^{m_3}(m_5\rho_2^{1-\beta}-C_1\rho_2^{m_1}-C_2\rho_2^{m_2})k_1}{-\rho_2^{m_3}b^{m_4}k_2+\rho_2^{m_4}b^{m_3}k_1}\right)k_2 r^{\beta+m_4-1}+k_3 \tag{54}$$

$$\sigma_\theta^p(r)=\left(\frac{-b^{1-\beta}\rho_2^{m_4}k_3+b^{m_4}(m_5\rho_2^{1-\beta}-C_1\rho_2^{m_1}-C_2\rho_2^{m_2})k_2}{-\rho_2^{m_3}b^{m_4}k_2+\rho_2^{m_4}b^{m_3}k_1}\right)k_4 r^{\beta+m_3-1}+\left(\frac{b^{1-\beta}\rho_2^{m_3}k_3-b^{m_3}(m_5\rho_2^{1-\beta}-C_1\rho_2^{m_1}-C_2\rho_2^{m_2})k_1}{-\rho_2^{m_3}b^{m_4}k_2+\rho_2^{m_4}b^{m_3}k_1}\right)k_5 r^{\beta+m_4-1}+k_6 \tag{55}$$

Using the stress continuity condition $\sigma_r^e(\rho_2)=\sigma_r^p(\rho_2)$, one obtains

$$p=\frac{g_1\rho_2^{\beta+m_1-1}c_1+g_2\rho_2^{\beta+m_2-1}c_2-k_3-c_3k_1\rho_2^{\beta+m_3-1}-c_4k_2\rho_2^{\beta+m_4-1}}{c_{30}k_1\rho_2^{\beta+m_3-1}+c_{40}k_2\rho_2^{\beta+m_4-1}+g_1\rho_2^{\beta+m_1-1}c_{10}-g_2\rho_2^{\beta+m_2-1}c_{20}} \tag{56}$$

where

$$c_3 = \frac{-b^{1-\beta}\rho_2^{m_4}k_3 + b^{m_4}k_2m_5\rho_2^{1-\beta} - b^{m_4}k_2\rho_2^{m_1}c_1 - b^{m_4}k_2\rho_2^{m_2}c_2}{-\rho_2^{m_3}b^{m_4}k_2 + \rho_2^{m_4}b^{m_3}k_1},$$
$$c_{30} = \frac{b^{m_4}k_2\rho_2^{m_1}c_{10} - b^{m_4}k_2\rho_2^{m_2}c_{20}}{-\rho_2^{m_3}b^{m_4}k_2 + \rho_2^{m_4}b^{m_3}k_1},$$
$$c_4 = \frac{b^{1-\beta}\rho_2^{m_3}k_3 - b^{m_3}k_1m_5\rho_2^{1-\beta} + b^{m_3}k_1\rho_2^{m_1}c_1 + b^{m_3}k_1\rho_2^{m_2}c_2}{-\rho_2^{m_3}b^{m_4}k_2 + \rho_2^{m_4}b^{m_3}k_1}, \quad (57)$$
$$c_{40} = \frac{-b^{m_3}k_1\rho_2^{m_1}c_{10} + b^{m_3}k_1\rho_2^{m_2}c_{20}}{\rho_2^{m_4}b^{m_3}k_1 - \rho_2^{m_3}b^{m_4}k_2}$$

3.4. Solutions to Case D

The fully plastic deformation is discussed here. Conversely, in Case B, full plasticity is initiated when $\rho_1 = b$. By substituting $\rho_1 = b$ into Eq. (44), the critical load can be determined as follows

$$p_s^B = \frac{g_1 b^{\beta+m_1-1}C_1^{(b)} + g_2 b^{\beta+m_2-1}C_2^{(b)} - c_3^{(b)}k_1 b^{\beta+m_3-1} - c_4^{(b)}k_2 b^{\beta+m_4-1} - k_3}{\frac{a^{1-\beta}k_2b^{\beta+m_3+m_4-1} - a^{1-\beta}k_1b^{\beta+m_3+m_4-1}}{b^{m_4}a^{m_3}k_1 - b^{m_3}a^{m_4}k_2}} \quad (58)$$

where

$$C_1^{(b)} = \frac{g_2 b^{1+m_2-\beta}Y_0}{b^{m_1+m_2}\left(g_1(g_2-g_4) - g_2(g_1-g_3)\right)},$$
$$C_2^{(b)} = -\frac{g_1 b^{m_1}b^{1-\beta}Y_0}{b^{m_1+m_2}\left(g_1(g_2-g_4) - g_2(g_1-g_3)\right)}, \quad (59a)$$

$$c_3^{(b)} = \frac{-b^{m_4}a^{1-\beta}k_3 + k_2a^{m_4}\left(m_5b^{1-\beta} - C_1^{(b)}b^{m_1} - C_2^{(b)}b^{m_2}\right)}{b^{m_4}a^{m_3}k_1 - b^{m_3}a^{m_4}k_2},$$
$$c_4^{(b)} = \frac{b^{m_3}a^{1-\beta}k_3 - k_1a^{m_3}\left(m_5b^{1-\beta} - C_1^{(b)}b^{m_1} - C_2^{(b)}b^{m_2}\right)}{b^{m_4}a^{m_3}k_1 - b^{m_3}a^{m_4}k_2} \quad (59b)$$

In Case C, by substituting $\rho_2 = a$ in Eq. (56), the critical load can be also determined as follows

$$p_s^C = \frac{g_1 a^{\beta+m_1-1}c_1^{(a)} + g_2 a^{\beta+m_2-1}c_2^{(a)} - k_3 - c_3^{(a)}k_1 a^{\beta+m_3-1} - c_4^{(a)}k_2 a^{\beta+m_4-1}}{c_{30}^{(a)}k_1 a^{\beta+m_3-1} + c_{40}^{(a)}k_2 a^{\beta+m_4-1} + g_1 a^{\beta+m_1-1}c_{10}^{(a)} - g_2 a^{\beta+m_2-1}c_{20}^{(a)}} \quad (60)$$

where

$$c_1^{(a)} = \frac{a^{m_2+1-\beta}g_2Y_0}{a^{m_1+m_2}\left(g_1(g_2-g_4) - g_2(g_1-g_3)\right)},$$
$$c_{10}^{(a)} = \frac{a^{m_2+1-\beta}(g_2-g_4)}{a^{m_1+m_2}\left(g_1(g_2-g_4) - g_2(g_1-g_3)\right)}, \quad (61a)$$

$$c_2^{(a)} = \frac{-a^{m_1+1-\beta}g_1Y_0}{a^{m_1+m_2}\left(g_1(g_2-g_4) - g_2(g_1-g_3)\right)},$$
$$c_{20}^{(a)} = \frac{a^{m_1+1-\beta}(g_1-g_3)}{a^{m_1+m_2}\left(g_1(g_2-g_4) - g_2(g_1-g_3)\right)}, \quad (61b)$$

$$c_3^{(a)} = \frac{-b^{1-\beta}a^{m_4}k_3 + b^{m_4}k_2m_5a^{1-\beta} - b^{m_4}k_2a^{m_1}c_1 - b^{m_4}k_2a^{m_2}c_2}{a^{m_4}b^{m_3}k_1 - a^{m_3}b^{m_4}k_2},$$
$$c_{30}^{(a)} = \frac{b^{m_4}k_2a^{m_1}c_{10} - b^{m_4}k_2a^{m_2}c_{20}}{a^{m_4}b^{m_3}k_1 - a^{m_3}b^{m_4}k_2}, \quad (61c)$$

$$c_4^{(a)} = \frac{b^{1-\beta}a^{m_3}k_3 - b^{m_3}k_1m_5a^{1-\beta} + b^{m_3}k_1a^{m_1}c_1 + b^{m_3}k_1a^{m_2}c_2}{a^{m_4}b^{m_3}k_1 - a^{m_3}b^{m_4}k_2},$$
$$c_{40}^{(a)} = \frac{-b^{m_3}k_1a^{m_1}c_{10} + b^{m_3}k_1a^{m_2}c_{20}}{a^{m_4}b^{m_3}k_1 - a^{m_3}b^{m_4}k_2} \quad (61d)$$

The critical load of fully plastic deformation is

$$p_s = \max\{p_s^B, p_s^C\} \quad (62)$$

Then, the exact solutions for p_e of Eq. (33) and p_s of Eq. (62) in the different states and displacement solutions of Eqs. (28), (36), (41), (48), (53) and stresses solutions of Eqs. (29)-(30), (37)-(38), (42)-(43), (49)-(50), (54)-(55) of the FGMs spherical shell can be given. The analytical solutions derived in this study systematically characterize the displacement and stress distributions of FGMs spherical shell under linear hardening elastoplastic conditions. Three key influencing factors are quantitatively analyzed: internal pressure, material gradient parameter, and elastic modulus variation. This research primarily employs Python for analytical solution computation and data processing.

4. Numerical verifications

The theoretical derivation is validated by comparing it with established solutions from existing references.

4.1. Elastic region verification

In Case A, the results obtained in this study are compared with those presented in Ref. [8]. As illustrated in Fig. 3, the radial and circumferential stresses distributions for the FGMs spherical shell align closely with the findings in Ref. [8], thereby validating the derivation of stresses in Case A. It's worth noting that the parameters considered are the same as in Ref. [8] when $E_1 = 0$ GPa.

4.2. Elastoplastic region verification

In the context of solutions in the plastic deformation region, one analyses the degradation results in this paper in comparison with theoretical solutions presented in Ref. [61]. When $\beta = 0$, the problem under investigation reduces to an elastoplastic solution for a hollow spherical shell composed of homogeneous materials, as outlined in Ref. [61]. As evidenced in Fig. 4(a) and 4(b), the findings from this study are quite the same as the solutions previously reported in Ref. [61]. Furthermore, Fig. 4 illustrates that under the given loading conditions, plastic deformation in a homogeneous spherical shell initiates at the inner diameter and subsequently propagates radially outward. It's worth noting that the parameters utilized in this analysis align with those specified in Ref. [61] and $E_0 = 200$ GPa, $E_1 = 220$ GPa, $Y_0 = 300$ MPa, and $\beta = 0$.

Furthermore, the extent of the elastoplastic deformation region is influenced by both internal pressure p and the gradient parameter β. Tables 1 and 2 present a comparative analysis of deformation states under varying internal pressure and the gradient parameter β, juxtaposed with results based on Ref. [59]. The yield strength is $Y(r) = Y_0(r/b)^{\alpha}$, where Y_0 is the yield strength and α is the gradient parameter in Ref. [59]. The parameters employed are set as $a = 0.6$ m, $b = 1$ m, $Y_0 = 100$ MPa, $E_0 = 300$ GPa, $\nu = 0.3$ and $E_1 = 0$ GPa. Table 1 indicates that for FGMs spherical shell, when $\beta = -2$, an increase in internal pressure leads to a sequence of deformation states: Cases A, B and D. In Table 2, at an internal pressure of $p = 50$ MPa, an increase in β transitions the FGMs spherical shell through Cases B, A, and C. The findings in Tables 1 and 2 demonstrate a consistent deformation state for the FGMs spherical shell between this study and Ref. [59]. Notably, the coordinates ρ are in close agreement with results in Ref. [59]. The difference (Δ) is defined as $\Delta = |\rho_{\text{now}} - \rho_{\text{previous}}|/\rho_{\text{now}} \times 100\%$.

5. Numerical discussions

These subsequent results and analyses elucidate the influence of p and β on the linear hardening elastoplastic model in FGMs spherical shell, where $a = 0.6$ m, $b = 1$ m, $\nu = 0.3$.

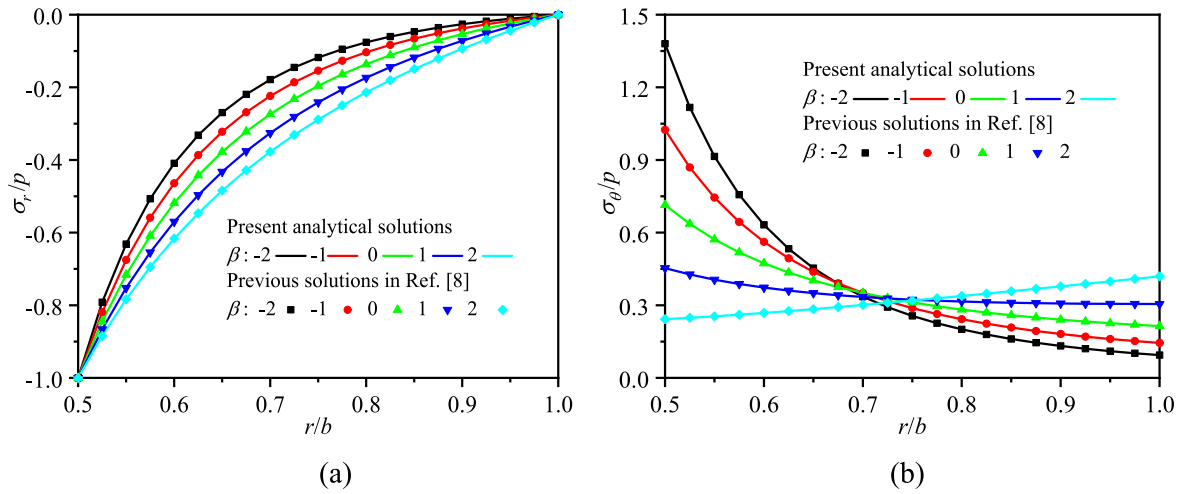

Fig. 3. Comparison of two results for stress distributions.

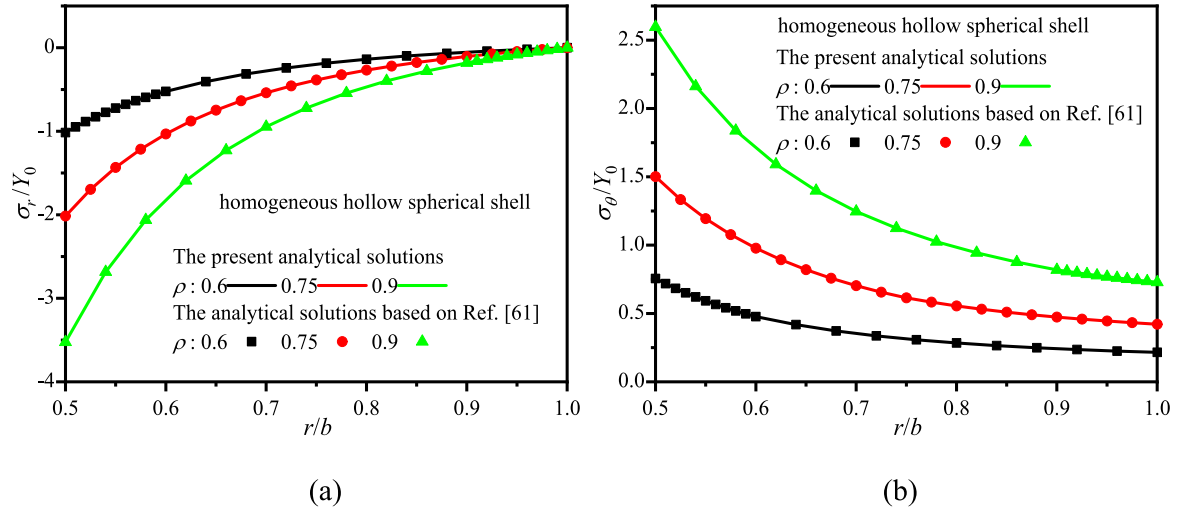

Fig. 4. Comparison of two results for stress distributions.

Table 1
A comparison of the deformation state of the FGMs spherical shell for different internal pressures with previous results in Ref. [59].

Previous results in Ref. [59]			Present results in this paper			difference (Δ)
α =0, β =-2			$E_1 = 0$, $\beta = -2$			
p (MPa)	Cases	ρ (m)	p (MPa)	Cases	ρ (m)	
10	A	–	10	A	–	–
30	A	–	30	A	–	–
50	B	0.637743	50	B	0.637660	0.0130 %
80	B	0.770712	80	B	0.770564	0.0192 %
100	B	0.932582	100	B	0.932556	0.0028 %
120	D	1.000000	120	D	1.000000	0.0000 %

Table 2
A comparison of the deformation state of the FGMs spherical shell for different gradient parameters with previous results in Ref. [59].

Previous results in Ref. [59]			Present results in this paper			difference (Δ)
α =0, p = 50 MPa			$E_1 = 0$, p = 50 MPa			
β	Case	ρ (m)	β	Case	ρ (m)	
−5	B	0.677594	−5	B	0.677516	0.0115 %
−1	B	0.617393	−1	B	0.617304	0.0144 %
0	A	–	0	A	–	–
1	A	–	1	A	–	–
5	A	–	5	A	–	–
10	C	0.9675736	10	C	0.967580	0.0007 %

5.1. Critical load and elastoplastic interface

The initial yield critical load p_e and critical load p_s of fully plastic deformation are influenced by the gradient parameter, geometric dimension, and yield strength. Fig. 5 illustrates the influence of the varying gradient parameter and yield strength on initial yield critical pressure p_e and full yield critical pressure p_s with E_0 = 300 GPa. A detailed analysis of p_e and p_s is presented. When the pressure p on the inner surface of the FGMs spherical shell exceeds p_e but remains below p_s, the structure enters a state of partial plastic and elastic deformation (Cases B or C). Conversely, with p surpassing p_s, the structure experiences full plastic deformation (Case D). As shown in Fig. 5(a), for a given Y_0, the p_e exhibits a nonlinear trend of gradual increase with the increase of gradient parameter. This nonlinear behavior is attributed to the shift of the initial yield position from the inner surface to the outer surface of the FGMs spherical shell as β increased. Fig. 5 shows that as β increases, p_s^B decreases and p_s^C increases gradually. In addition, as the E_1 increases, p_s^B decreases but p_s^C increases.

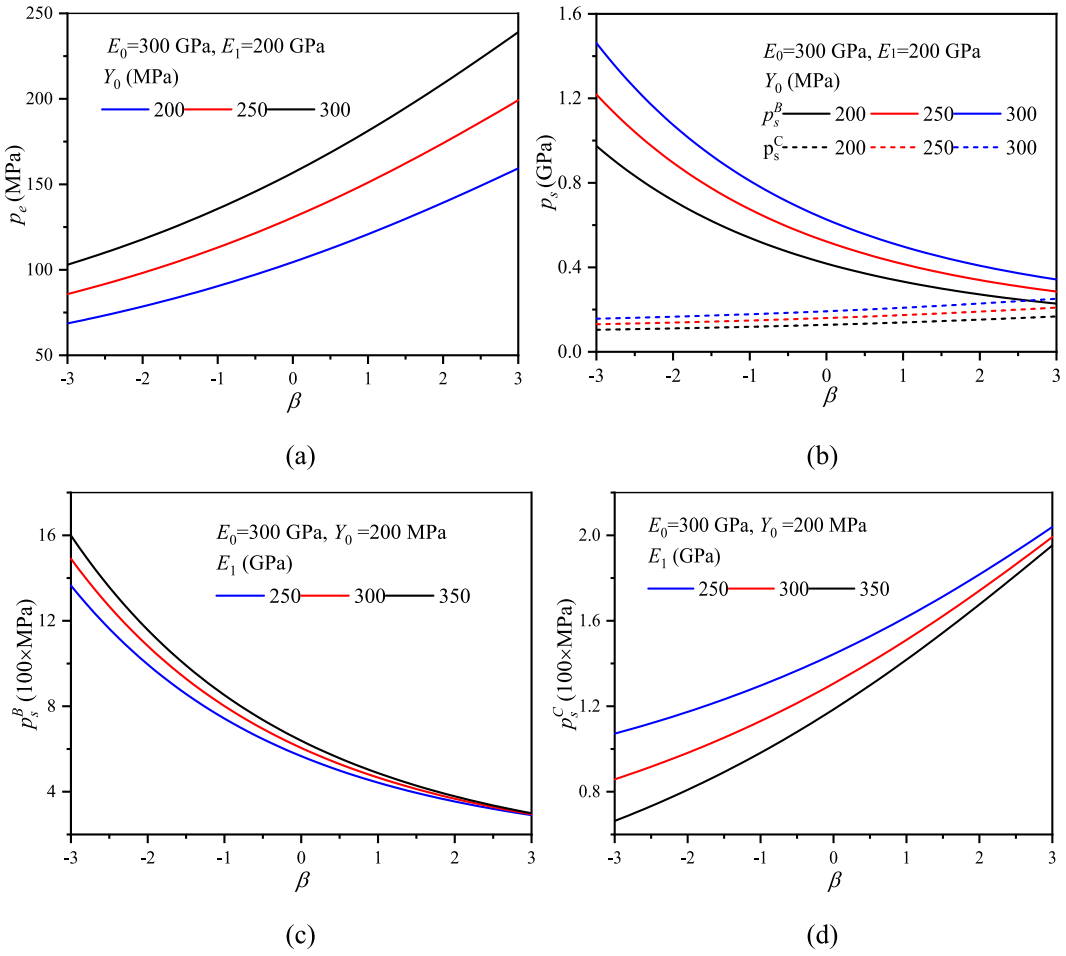

Fig. 5. The influence of β and Y_0 on critical pressure values.

The radial coordinates marking the interface between the elastic and plastic deformation regions are inherently influenced by both the internal pressure and the gradient parameter. This subsection examines the impact of these factors on the size of the elastoplastic deformation region.

Table 3 presents the influence of p and β on deformation states and interface ρ of the FGMs spherical shell. The parameters selected are $Y_0 =$ 100 MPa, $E_0 = 300$ GPa, $E_1 = 200$ GPa. From Table 3, it is evident that for the FGMs sphere, an increase in p results in a sequence of deformation states: elastic deformation (Case A), followed by partial plastic deformation (Case B), and ultimately leading to full plastic deformation (Case D) when $\beta = -2$. Additionally, as β increases, the FGMs spherical shell exhibits a sequence of deformation states at an internal pressure of $p = 50$ MPa, and the deformation states of the FGMs spherical shell are Cases A, C, and D in that order.

A detailed analysis is conducted on the critical loads corresponding to pure elastic and partial plastic deformation states that may occur in FGMs spherical shell. When the pressure is below the initial yield critical load p_e, the FGMs spherical shell remains in a purely elastic deformation state. For pressures greater than p_e but less than the critical load of fully plastic deformation p_s, the shell experiences partial plastic deformation. When the pressure reaches p_s, the shell enters a fully plastic deformation state.

Table 3
The state of FGMs spherical shell for different internal pressures and the gradient parameter.

β=-2			p = 50 MP		
p (MPa)	Case	ρ (m)	β	Case	ρ (m)
10	A	–	−5	B	0.657056
30	A	–	−1	B	0.616496
50	B	0.633544	0	A	–
80	B	0.708144	1	A	–
100	B	0.747164	5	A	–
120	B	0.780480	10	C	0.970620
350	D	1.000000	15	C	0.942608

5.2. Effect of internal pressure

Herein, one considers the influence of elastic modulus on the displacement and stresses distributions.

Fig. 6 depicts the influence of p on the deformation behavior within FGMs spherical shell where $Y_0 = 200$ MPa, $E_0 = 300$ GPa, $E_1 = 200$ GPa. For a given $p \in [0, 300$ MPa] and $\beta \in [-5, 5]$, the deformation state can be evaluated from Fig. 6(a). When the β and p values fall within the region indicated by blue points, the FGMs structure state is Case A. If the parameter values lie within the region marked by green points, the FGMs structure state is Case B. Conversely, when the β and p values correspond to the region represented by black points, the FGMs structure state is Case D. Notably, under the current loading conditions and gradient parameters, there is no observed Case C. The behaviors associated with the blue, green, and black points regions in Figs. 7 and 8 are consistent with those in Fig. 6(a). Specifically, for $p \in [0, 300$ MPa], and $\beta \in [-5, 5]$, the dominant deformation state is Case B. For $-5 \leq \beta < 1$, an increase in internal pressure p transitions the deformation state from Cases A to B. In the range $1 \leq \beta < 3$, the deformation states progress sequentially from Cases A to B and ultimately to D as internal pressure increases. For $3 \leq \beta \leq 5$, as internal pressure p increases, the deformation states transition

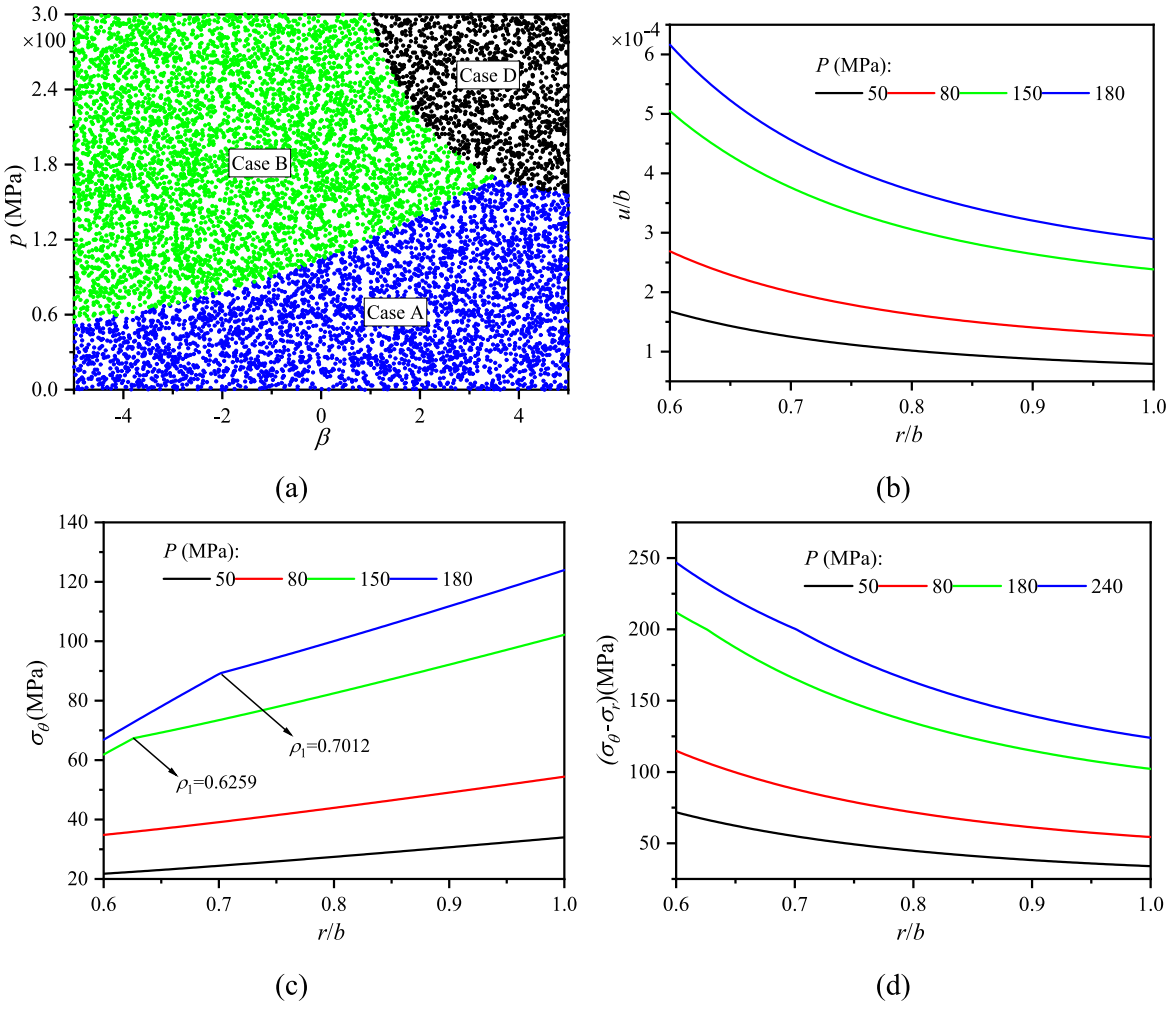

Fig. 6. The influence of internal pressure on the elastoplastic behavior.

from Cases A to D. Fig. 6(b)-(d) present the displacement, circumferential stress, and the difference between radial and circumferential stresses for β =2 at internal pressures of 50, 80, 150, and 180 MPa, respectively. The results indicate that as p increases, the FGMs structure transitions from elastic (Case A) to partial plastic deformation (Case B). Specifically, at $p = 150$ MPa and $p = 180$ MPa, the radial displacement values are $\rho_1 = 0.6259$ m and 0.7012 m, respectively. Further increases in internal pressure result in the FGMs structure entering a state of full plastic deformation, which is corroborated by the observations in Fig. 6 (a).

5.3. Effect of elastic modulus

Herein, one considers the influence of elastic modulus on the displacement and stresses distributions.

Fig. 7 shows the elastic modulus E_1 influence on the deformation behavior, where $Y_0 = 200$ MPa, $E_0 = 300$ GPa, $\beta = 0.2$ and $E_1 = 150$ GPa for Fig. 7(b)-(d). Fig. 7(a) illustrates the influence of p on the elastoplastic state diagram of the FGMs structure. It is observed that for $p \in [0, 300$ MPa], and $E_1 \in [0, 300$ GPa], the predominant state of FGMs structure is Case A. Specifically, for $0 \le p < 146$ MPa, the shell exhibits Case A deformation. For 146 MPa $\le p \le 191$ MPa, it transitions to Case B, and for $p > 191$ MPa, the spherical shell experiences full plastic deformation. Fig. 7(b)-(d) illustrate the displacement, circumferential stress, and the difference between radial and circumferential stresses for $E_1 = 150$ GPa. As indicated in Fig. 7(b), displacement increases with the increase of internal pressure p, with a transition from elastic to partial plastic deformations (Case B) occurring at $p = 150$ MPa and $p = 180$ MPa. The radial coordinates $\rho_1 = 0.6259$ m and 0.7012 m. As the internal pressure increases further, the FGMs spherical shell enters into full plastic deformation. This can also be verified from Fig. 7(a) further.

5.4. Effect of gradient parameter

Herein, one considers the effect of the gradient parameter on displacement and stresses distributions of the FGMs spherical shell.

Fig. 8 shows the influence of β on the deformation behavior where $Y_0 = 200$ MPa, $E_0 = 300$ GPa, $\nu = 0.3$, and $p = 140$ MPa for Fig. 8(b)-(d). When the β and p values fall within the region indicated by red points, the FGMs structure state is Case C. It can be seen from Fig. 8(a) that when $p \in [0, 300$ MPa], and $\beta \in [-4, 8]$, a large portion of the points in Fig. 8(a) fall in the blue and green regions, implying that a large portion of the interior of the FGMs structure is in the deformed state of Cases A and B. When $-4 \le \beta < 3.2$, the states transition from Cases A to B as the p increases. When $3.2 \le \beta < 4.1$, the states transition from Cases A to B and D in turn as the p increases. When $4.1 \le \beta \le 8$, the states transition from Cases A to C and D in turn. When $p = 140$ MPa, Fig. 8(b)-(d) show the displacement, the circumferential stress, and the difference between radial and circumferential stresses of the FGMs spherical shell. From Fig. 8(b), the displacement increases with increasing internal pressure p. It is clear that for $\beta = 2$, 4 and 7, the FGMs spherical shell exhibits a transition from elastic to partial plastic deformations (Cases B and C) at the respective radial coordinates of $\rho_1 = 0.6017$ m, 0.6858 m and 0.9559 m. With the progressive increase in load p, the structure

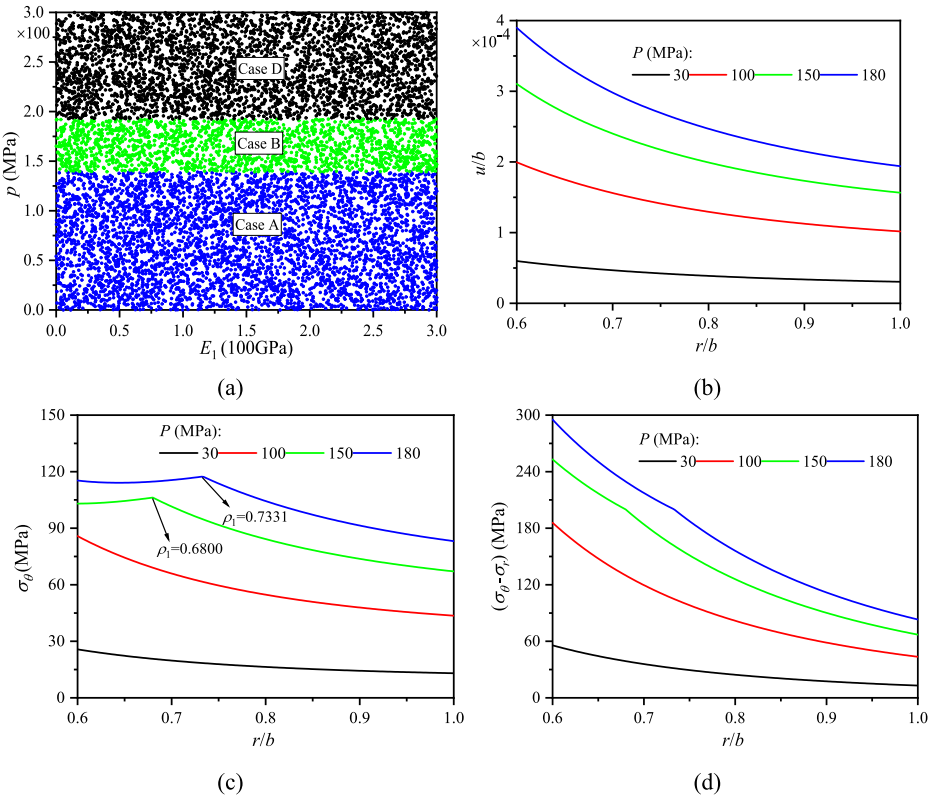

Fig. 7. The influence of elastic modulus E_1 on the elastoplastic behavior.

ultimately enters a state of full plastic deformation. Furthermore, this change in stress distribution with increasing β results in a shift of the yield location from the inner to outer surfaces of the FGMs structure.

5.5. Deformation state determination and applications

Herein, the deformation state determination based on critical loads and practical implications of the results are given.

This study proposes a systematic analytical solution method for analyzing the deformation behavior of FGMs spherical shell under different internal pressure loads. Based on given material parameters and gradient parameters, by inputting the internal pressure p and comparing it with critical load values (initial yield critical load p_e and fully plastic deformation critical load p_s), the current deformation state of the structure can be precisely determined. When $p < p_e$, the spherical shell remains in a purely elastic deformation state; when $p_e \le p < p_s$, the spherical shell undergoes partial plastic deformation; when $p \ge p_s$, the spherical shell enters a fully plastic deformation state. For each deformation state, the corresponding analytical solutions for displacement and stress are derived. As shown in Fig. 9, the flowchart for deformation state judgment and displacement and stresses distributions analysis based on the analytical solutions is presented. The classification of four typical deformation states deepens the understanding of structural deformation and even damage mechanisms. The proposed method not only serves as a theoretical framework for predicting the mechanical behavior of FGMs spherical shell but also offers significant practical value in engineering applications, such as pressure vessel design. For instance, in pressure vessel optimization, the analytical solutions can guide the selection of material parameters and gradient designs, thereby enhancing the load-bearing capacity and operational lifespan of the vessels.

6. Conclusion

The exact solutions for the linear hardening elastoplastic model in FGMs spherical shell are studied using the small deformation theory in this paper. The following conclusions can be drawn:

1. The critical pressure values between different deformation states containing pure elasticity, partial plasticity and fully plasticity are obtained for the FGMs spherical shell. Based on any given value combination of internal pressure, one can use the analytical expression for the critical load of Eqs. (33), (58) and (60) to determine the deformation state of the spherical shell.
2. The exact solutions of the stresses and displacement in the FGMs spherical shell are obtained. When the elastic state of the FGMs spherical shell is determined under a given load, the displacement and stresses distributions at each position of the spherical shell can be calculated from the exact expressions for different deformation states given analytically.
3. The study reveals that the deformation behavior of FGMs spherical shell is significantly influenced by internal pressure p, gradient parameter β, and elastic modulus E_1. As the internal pressure increases, the deformation state transitions progressively from elastic (Case A) to partial plasticity (Case B) and full plasticity (Case D), with the transition path varying across different ranges of β.
4. The elastic modulus E_1 significantly affects the deformation state, with lower E_1 values more likely to induce plastic deformation. The study also finds that as β increases, the yield location shifts gradually from the inner to the outer surface of the spherical shell, further highlighting the complex influence of gradient parameters on the mechanical behavior.

Furthermore, the research presented in this paper can be further expanded. Many FGMs exhibit nonlinear hardening behavior [62,63] due to their composite nature, and exploring additional nonlinear

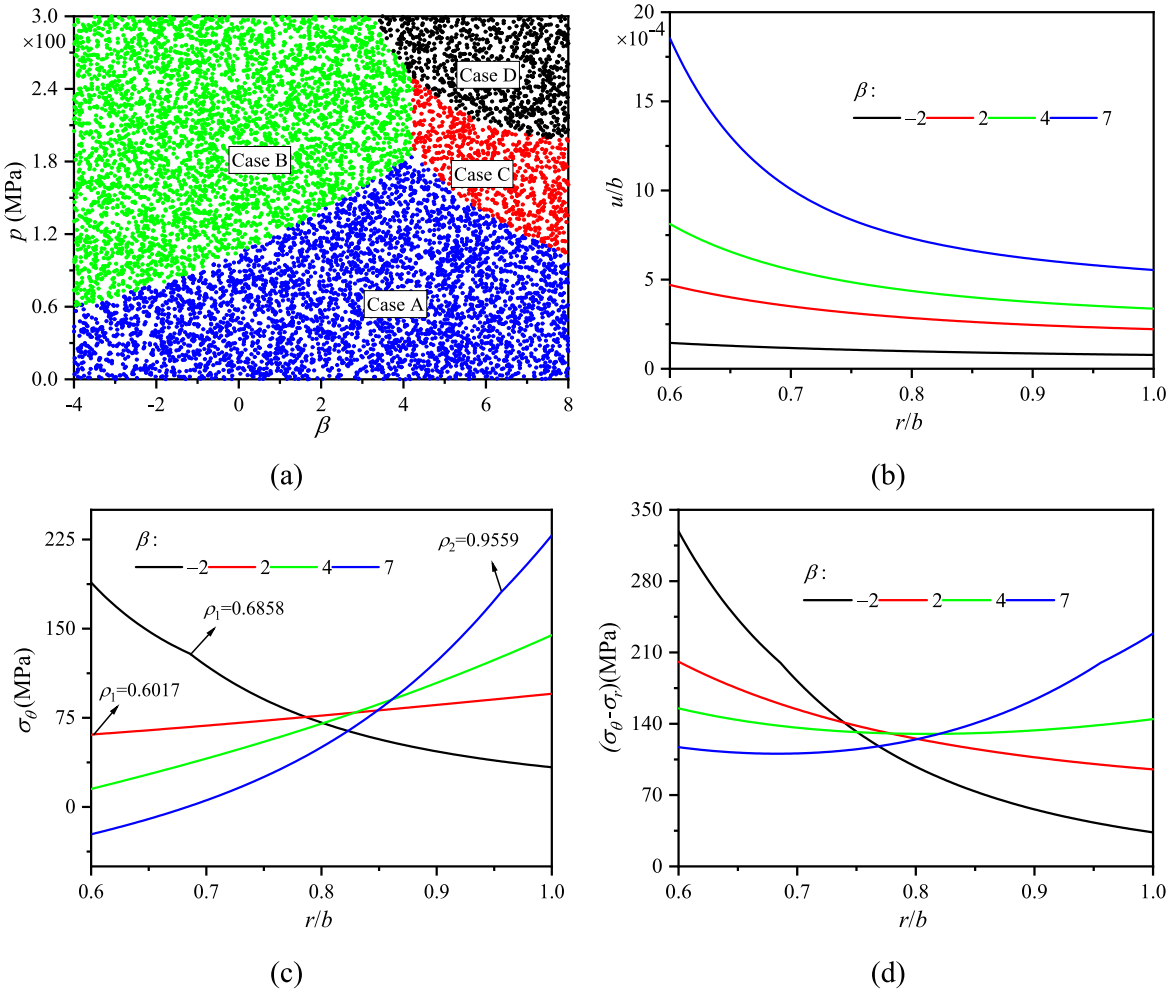

Fig. 8. The influence of gradient parameter β on the elastoplastic behavior.

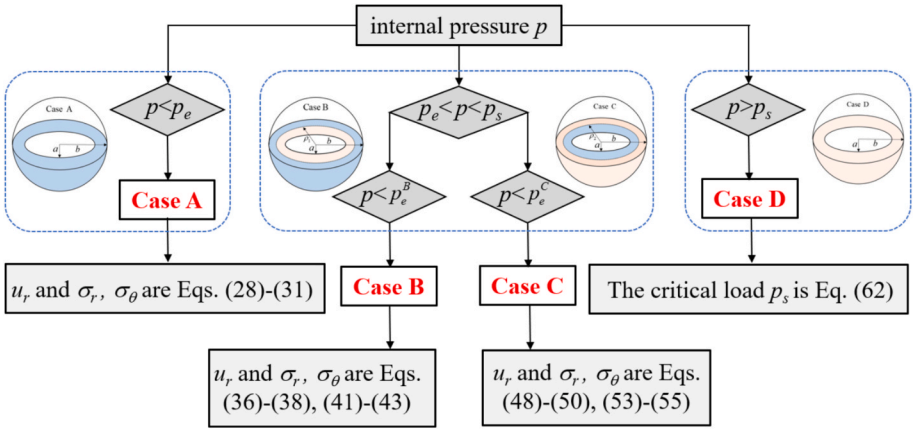

Fig. 9. Flowchart of deformation state judgement and displacement and stresses calculation of FGMs spherical shell.

hardening models could provide further insights. The solutions derived here can also be extended to more complex loading conditions, such as combinations of internal and external pressures or displacement boundary conditions [10,11]. Additionally, one aims to investigate other laws distribution [28] of FGMs to validate and broaden the scope of our findings.

CRediT authorship contribution statement

Jun Xie: Writing – review & editing, Writing – original draft, Software, Methodology, Formal analysis. **Xiaofan Gou:** Visualization, Supervision, Methodology, Funding acquisition, Data curation. **Pengpeng Shi:** Validation, Software, Resources, Formal analysis, Data curation.

Declaration of competing interest

The authors declare that they have no known competing financial interests or personal relationships that could have appeared to influence the work reported in this paper.

Acknowledgments

This work was supported by the Fundamental Research Funds for the Central Universities (No. B250201171), the National Natural Science Foundation of China (Nos. 12232005 and 12072101) and the Ningxia Natural Science Foundation of China (Nos. 2024AAC04004 and 2024AAC03412). Authors gratefully acknowledge these financial supports.

Data availability

Data will be made available on request.

References

[1] Ram SC, Bhushan A, Kumar MR, et al. A comparative study of processing route, microstructures, fracture analysis and phase formation of Al-Si/Mg_2Si functionally graded composites: an overview. COMPOS INTERFACE 2024;31(12):1575–614.
[2] Devesh P, Tarun K. A critical review of stress and vibration analyses of functionally graded shell structures. COMPOS STRUCT 2019;210:787–809.
[3] Boggarapu V, Gujjala R, Ojha S, et al. State of the art in functionally graded materials. COMPOS STRUCT 2021;262:113596.
[4] Horgan CO, Chan AM. The pressurized hollow cylinder or disk problem for functionally graded isotropic linearly elastic materials. J ELASTICITY 1999;55(1):43–59.
[5] Tutuncu N, Murat O. Exact solutions for stresses in functionally graded pressure vessels. COMPOS PART B-ENG 2001;32(8):683–6.
[6] Nejad MZ, Abedi M, Lotfian MH, et al. Exact and numerical elastic analysis for the FGM thick-walled cylindrical pressure vessels with exponentially-varying properties. Arch Metall Mater 2016;61(3):1649–54.
[7] Shi PP, Xie J. Revisiting classic problems of exact solutions for stresses in functionally graded pressure vessels. MECH RES COMMUN 2020;20:103609.
[8] Xie J, Hao S, Wang WS, et al. Analytical solution of stress in functionally graded cylindrical/spherical pressure vessel. ARCH APPL MECH 2021;35(04):3341–63.
[9] Shi ZF, Zhang TT, Xiang HJ. Exact solutions of heterogeneous elastic hollow cylinders. COMPOS STRUCT 2007;79(1):140–7.
[10] Shi PP, Xie J, Li X. Multilayer heterostructure inhomogeneous model for pressurized functionally graded annular structures (cylinder/sphere/annulus) with arbitrary elastic property along the radial direction. COMPOS STRUCT 2023;322:117425.
[11] Xie J, Li H, Li FJ, et al. Multilayer heterostructure inhomogeneous model for the functionally graded spherical shell with rotation effect for arbitrarily varying material properties. COMPOS STRUCT 2024;339:118145.
[12] Li XF, Peng XL, Kang YA. Pressurized hollow spherical vessels with arbitrary radial nonhomogeneity. AIAA J 2009;47:2262–5.
[13] Chen YZ, Lin XY. An alternative numerical solution of thick-walled cylinders and spheres made of functionally graded materials. COMP MATER SCI 2010;48(3):640–7.
[14] Wang GN, Dong LT, Atluri SN. Direct and inverse multi-scale analyses of arbitrarily functionally graded layered hollow cylinders (discs), with different shaped reinforcements, under harmonic loads. COMPOS STRUCT 2018;188:425–37.
[15] Horgan CO, Chan AM. The stress response of functionally graded isotropic linearly elastic rotating disks. J ELASTICITY 1999;55(3):219–30.
[16] Nejad MZ, Rahimi GH. Elastic analysis of FGM rotating cylindrical pressure vessels. J CHIN INST ENG 2010;33(4):525–30.
[17] Zenkour AM, Elsibai KA, Mashat DS. Elastic and viscoelastic solutions to rotating functionally graded hollow and solid cylinders. APPL MATH MECH-ENGL 2008;29(12):1601–16.
[18] Bayat M, Saleem M, Mahdi E. Analysis of functionally graded rotating disks with variable thickness. MECH RES COMMUN 2008;35(5):283–309.
[19] Wang HM. Effect of material inhomogeneity on the rotating functionally of a graded orthotropic hollow cylinder. J MECH SCI TECHNOL 2010;24(9):1839–44.
[20] Jabbari M, Sohrabpour S, Eslami MR. Mechanical and thermal stresses in a functionally graded hollow cylinder due to radially symmetric loads. INT J PRES VES PIP 2002;79:493–7.
[21] Jabbari M, Sohrabpour S, Eslami MR. General solution for mechanical and thermal stresses in a functionally graded hollow cylinder due to no axisymmetric steady-state loads. INT J APPL MECH 2003;70:111–8.
[22] Li H, Xie J, Wang WS, et al. Multilayer heterostructure inhomogeneous model for thermoelastic analysis of the functionally graded cylinder with arbitrary elastic property along the radial direction. APPL MATH MODEL 2025;141:115924.
[23] Kordkheili SA, Naghdabadi R. Thermoelastic analysis of functionally graded cylinders under axial loading. J THERM STRESSES 2008;31(1):1–17.
[24] Peng XL, Li XF. Thermoelastic analysis of a cylindrical vessel of functionally graded materials. INT J PRES VES PIP 2010;87(5):203–10.
[25] Li X, Xie J, Shi PP. Magneto-thermal-mechanical analysis of functionally graded material cylinder. ARCH APPL MECH 2022;93(4):1449–57.
[26] Gharooni H, Ghannad M. Nonlinear analysis of radially functionally graded hyperelastic cylindrical shells with axially-varying thickness and non-uniform pressure loads based on perturbation theory. J COMPUT APPL MECH 2019;50(2):324–40.
[27] Zhang YC, Cai J, Cai Q, et al. Strength and energy absorption characteristic of nanoparticle-reinforced composites considering interface curvature dependence. COMPOS STRUCT 2025;360:119036.
[28] Shi PP, Xie J, Li H, et al. Symmetric deformation of functionally graded annular structures with arbitrarily varying material properties: Operator discrete approximation for variable coefficient ordinary differential equation model. Thin-Walled Struct 2025;209:112911.
[29] Saadatfar M. Transient response of a hollow functionally graded piezoelectric cylinder subjected to coupled hygrothermal loading. INT J APPL MECH 2021;13(10):2150109.
[30] Yaghoobi MP, Ghaffari I, Ghannad M. Stress and active control analysis of functionally graded piezoelectric material cylinder and disk under electro-thermo-mechanical loading. J INTEL MAT SYST STR 2018;29(5):924–37.
[31] Mehditabar A, Rahimi GH, Tarahhomi MH. Thermo-elastic analysis of a functionally graded piezoelectric rotating hollow cylindrical shell subjected to dynamic loads. MECH ADV MATER STRUC 2018;25(12):1068–79.
[32] P.P. Shi, J. Xie, S, Hao. Static response of functionally graded piezoelectric-piezomagnetic hollow cylinder/spherical shells with axial/spherical symmetry, J MECH SCI TECHNOL. 35(4) (2021) 1583-1596.
[33] Dai T, Dai HL. Analysis of a rotating FGMEE circular disk with variable thickness under thermal environment. APPL MATH MODEL 2017;45:900–24.
[34] Chen WQ, Liu DY, Yang J. Bifurcation of pressurized functionally graded elastomeric hollow cylinders. COMPOS PART B-ENG 2017;109:259–76.
[35] Moosaie A. A nonlinear analysis of thermal stresses in an incompressible functionally graded hollow cylinder with temperature-dependent material properties. EUR J MECH A-SOLID 2016;55:212–20.
[36] Anani Y, Rahimi GH. Stress analysis of rotating cylindrical shell composed of functionally graded incompressible hyperelastic materials. INT J MECH SCI 2016;108:122–8.
[37] Jebellat E, Jebellat I. Stress analysis of functionally graded hyperelastic variable thickness rotating annular thin disk: A semi-analytic approach. MATER SCI+ 2024. 10.48550/arXiv.2404.11365.
[38] Turner LB. The stresses in a thick hollow cylinder subjected to internal pressure, transactions cambridge philosophical. Society 1910;21:377–96.
[39] Grave U. On the stress in an elastic-plastic annular disk of variable thickness under external pressure. INT J SOLIDS STRUCT 1993;30(5):651–8.
[40] Wang R, Xiong ZH, Huang WB. Fundamentals of Plastic Mechanics. Beijing: Science Press; 1982. in Chinese.
[41] You LH, Zhang JJ. Elastic-plastic stresses in a rotating solid disk. INT J MECH SCI 1999;41:269–82.
[42] Rees DW. Elastic-plastic stresses in rotating discs by von Mises and Tresca. ZAMM-Z ANGEW MATH ME 1999;79(4):281–8.
[43] Eraslan AN, Orcan Y. Elastic-plastic deformation of a rotating solid disk of exponentially varying thickness. MECH MATER 2002;34(7):423–32.
[44] Bektas NB. Elastic-plastic and residual stress analysis of a thermoplastic composite hollow disc under internal pressures. J THERMOPLAST COMPOS 2005;18(4):363–75.
[45] Alexandrov S, Jeng YR. An elastic/plastic solution for a hollow sphere subject to thermo-mechanical loading considering temperature dependent material properties. INT J SOLIDS STRUCT 2020;200:23–33.
[46] S. Sharma. Elastic-plastic transition of a non-homogeneous thick-walled circular cylinder under internal pressure, DEFENCE SCI J. 54(2) (2004).135-141.
[47] Gupta SK, Pathak S. Elastic-plastic transition in non-homogeneous thick-walled rotating cylinders. INDIAN J PURE AP MAT 1999;30(12):1297–309.
[48] Eraslan AN, Akis T. Plane strain analytical solutions for a functionally graded elastic-plastic pressurized tube. INT J PRES VES PIP 2006;83(9):635–44.
[49] Akis T, Eraslan AN. Exact solution of rotating FGM shaft problem in the elastoplastic state of stress. ARCH APPL MECH 2007;77:745–65.
[50] Akis T, Eraslan AN. The stress response and onset of yield of rotating FGM hollow shafts. Acta Mech 2006;187:169–87.
[51] Eraslan AN, Akis T. The stress response of partially plastic rotating FGM hollow shafts: analytical treatment for axially constrained ends. MECH BASED DES STRUC 2006;34:241–60.
[52] Fatehi P, Nejad MZ. Effects of material gradients on onset of yield in FGM rotating thick cylindrical shells. INT J APPL MECH 2014;6(4):1450038.
[53] Shokrollahi H. Elastic-plastic analysis of functionally graded spherical pressure vessels using strain gradient plasticity. INT J APPL MECH 2017;9(8):1750118.
[54] Mohammad ZN, Negar A, Amin H. Thermoelastoplastic analysis of FGM rotating thick cylindrical pressure vessels in linear elastic-fully plastic condition. COMPOS PART B-ENG 2018;154:410–22.
[55] Sharma S, Yadav S. Thermo elastic–plastic analysis of rotating functionally graded stainless steel composite cylinder under internal and external pressure using finite difference method. ADV MATER SCI ENG 2013;81:810508.
[56] Hassani A, Hojjati MH, Farrahi G, et al. Semi-exact solution for thermo-mechanical analysis of FG elastic-strain hardening rotating disks. COMMUN NONLINEAR SCI 2012;17:3747–62.

[57] Atai AA, Lak D. Analytic investigation of effect of electric field on elasto-plastic response of a functionally graded piezoelectric hollow sphere. J MECH SCI TECHNOL 2016;30(1):113–9.
[58] Atai AA, Lak D. Analytic solution of effect of electric field on elasto-plastic response of a functionally graded piezoelectric hollow cylinder. INT J PRES VES PIP 2017; 155:1–14.
[59] Xie J, Shi PP, Li FJ. Exact solutions for the symmetric elastoplastic response of functionally graded pressure vessels. THIN WALL STRUCT 2023;192:111165.
[60] Shi PP, Xie J. Exact solution of magneto-elastoplastic problem of functionally graded cylinder subjected to internal pressure. APPL MATH MODEL 2023;123: 835–55.
[61] Xv BY, Huang Y, Liu XS. Elasticity and Plasticity Mechanics Solution Guide and Exercise Set. Beijing: Higher Education Press; 1985. in Chinese.
[62] Xiao G, Yang X, Qiu J, et al. Determination of power hardening elastoplastic constitutive relation of metals through indentation tests with plural indenters. MECH MATER 2019;138:103173.
[63] Jrad H, Mars J, Wali M, et al. Geometrically nonlinear analysis of elastoplastic behavior of functionally graded shells. ENG COMPUT-GERMANY 2019;35:833–47.